**Proceedings of GT2005**
**ASME Turbo Expo 2005: Power for Land, Sea and Air**
**June 6-9, 2005, Reno-Tahoe, Nevada, USA**

# GT2005-68839

# FINITE ELEMENT ANALYSIS OF COUPLED LATERAL AND TORSIONAL VIBRATIONS OF A ROTOR WITH MULTIPLE CRACKS

**Xi Wu**
Rotor-Bearing Dynamics & Diagnostics Laboratory
Cleveland State University
Cleveland, OH 44115-2214

**Jerzy T. Sawicki**
Rotor-Bearing Dynamics & Diagnostics Laboratory
Cleveland State University
Cleveland, OH 44115-2214

**Michael I. Friswell**
University of Bristol, Department of Aerospace Engineering, Bristol BS8 1TR, UK

**George Y. Baaklini**
NASA Glenn Research Center
21000 Brookpark Road, MS 77-1
Cleveland, OH 44135

## ABSTRACT

The coupling between lateral and torsional vibrations has been investigated for a rotor dynamic system with breathing crack model. The stiffness matrix has been developed for the shaft element which accounts for the effect of the crack and all six degrees of freedom per node. Since the off-diagonal terms of the stiffness matrix represent the coupling of the respective modes, the special attention has been paid on accurate determination of their values. Based on the concepts of fracture mechanics, the variation of the stiffness matrix over the full shaft revolution is represented by the truncated cosine series where the fitting coefficient matrices are extracted from the stiffness matrices of the cracked shaft for a number of its different angular positions. The variation of the system eigenfrequencies and dynamic response of the rotor with two cracks have been studied for various shaft geometries, crack axial locations, and relative phase of cracks.

## INTRODUCTION

Any new advancement in on-line detection and diagnosis of critical malfunctions in rotating machinery can be extremely beneficial to industry [1]. This especially applies to fatigue cracks on the shaft, which present a potential source for catastrophic failures of rotating machinery. Most reported studies are focused on two crack signatures, i.e., twice the running frequency component (2X) and the subharmonic component at approximately half of the shaft critical speed. A study done by Tondl [2] was one of the first to investigate the effect of the coupled lateral and torsional vibrations on turbogenerator rotor stability. He concluded that the combined effect of torsional stiffness and bending stiffness results in speed intervals where the rotor vibrations due to residual unbalance become unstable. A comprehensive literature review of various crack modeling techniques and system behavior of cracked rotor is given by Wauer [3]. Papadopoulos and Dimarogonas [4] used a non-rotating cracked Timoshenko shaft to demonstrate the existence of an apparent coupling of torsional and bending vibration. They modeled crack using the local flexibility matrix, and then proceeded to study the vibration spectra in the presence of harmonic excitations. Other researchers also dealt with the problem of coupled vibrations, for example Plaut and Wauer [5] investigated resonances and instabilities in coupled flexural and torsional vibrations of a rotating shaft. Muszynska et al. [6] analytically and experimentally analyzed lateral/torsional coupling mechanisms resulting from combinations of unbalance, shaft stiffness asymmetry, and radial sideload. Muszynska experimentally observed torsional resonance at speeds equal to 1/8, 1/6, 1/4, and 1/2 of the lowest torsional natural frequency. Bently et al. [7] continued this study with special attention paid to the analysis of a “snapping” action which occurs when during rotation the rotor experiences a peak torsional acceleration.

The topic of cracked rotor vibrations has been analyzed in a number of published works [8-16]. They have been focused on the study of dynamic behavior of rotors with the so-called breathing type of crack during the passage through the critical speed at the constant angular acceleration or deceleration. For example, Sawicki et al. [9, 10] studied the accelerating cracked rotor response using the angle between the crack centerline and the rotor whirl vector to determine the closing and opening of the crack. This allows one to study the rotor dynamic response with or without the rotor weight dominance by taking into account nonsynchronous whirl. Henry [11] investigated how the gravity and the unbalance affect the vibration response of a cracked shaft. A theoretical and experimental study of the effects of a transverse crack on the rotor dynamic system was

given by Mayes [12]. From the experimental results, it is observed that the crack has most significant effects on the response of the rotor dynamic system when the phase angle between unbalance and crack is in the range of 45° and 135°. Out of this range, the rotor behaves like an un-cracked rotor. Gash [13, 14] provided a comprehensive investigation of the stability behavior and insightful study of harmonic resonances of a cracked Jeffcott rotor with the hinge model of the crack. Mayes and Davies [15] modified hinge model to account for deep cracks, by introducing the crack cross flexibility. Collins et al. [16] used axial impulses for crack detection in rotating shafts.

Practical simulation of cracked rotordynamic systems calls for application of finite element analysis to account for geometric characteristics of the rotor. Papadopoulos and Dimarogonas [17] derived flexibility matrix for the shaft element with open crack. Later, they studied [18] coupling between bending, longitudinal and torsional modes of vibration for non-rotating shaft with an open crack. Sekhar [19] presented results of finite element analysis of the flexural vibration response of the cracked rotor with two open transverse cracks, focusing mainly on the stability study and eigenfrequency analysis. However, an open crack model in a case of rotating shaft is not practical. The rotor vibration characteristics with such crack model can be very different than with the breathing crack model. Darpe et al. [20] presented study of coupled longitudinal, lateral, and torsional vibrations for the cracked rotating shaft using a response-dependent non-linear breathing crack model. The signs of the overall stress intensity factors (SIF) at any point along the crack edge are used to judge whether the crack is open or close, thus determining the crack closure line position.

In this paper, the coupled lateral and torsional vibrations of a rotating shaft with two breathing cracks are investigated using the finite element approach. Based on the concepts of fracture mechanics, the variation of the stiffness matrix over one rotor revolution is expressed by the truncated cosine series, in which the fitting coefficient matrices are determined from the stiffness matrices of the cracked shaft at five different angular positions. The method accurately predicts not only the direct stiffness terms, but also the off-diagonal terms which account for coupling mechanisms of the respective modes. The developed approach accurately describes crack breathing action and can be effectively applied to the frequency analysis of the rotor with two cracks at two different angular and/or axial positions, and for different shaft geometric ratios. Coupled lateral and torsional vibrations of a rotating shaft with two breathing cracks of different relative phase, under unbalance, gravity and external torque excitations are studied.

## NOMENCLATURE

| | |
|---|---|
| $a$ | Depth of the crack |
| $\bar{a}$ | Normalized depth of the crack ( $a/R$ ) |
| $b$ | Half-width of the crack |
| $\bar{b}$ | Normalized half-width of the crack $\sqrt{2\bar{a}-\bar{a}^2}$ |
| $\mathbf{c}_c$ | Cracked element flexibility matrix |
| $\mathbf{C}$ | Global damping matrix |
| $D$ | Shaft diameter |
| $E$ | Modulus of elasticity |
| $\mathbf{F}$ | Global force vector |
| $G$ | Shear modulus of elasticity |
| $\mathbf{I}_{6\times6}$ | Identity matrix |
| $J$ | Strain Energy Density Function |
| $J_P$ | Polar moment of inertia |
| $J_D$ | Diametral moment of inertia |
| $\mathbf{k}_c$, $\mathbf{K}_c$ | Cracked element stiffness matrix in rotor-fixed and inertial coordinate systems, respectively |
| $\mathbf{K}(\omega t)$ | Global stiffness matrix |
| $l$ | Length of shaft element |
| $L$ | Length of rotor |
| $M$ | Disk mass |
| $\mathbf{M}$ | Global mass matrix |
| $\mathbf{q}$ | Displacement nodal vector |
| $R$ | Shaft radius |
| $t$ | Instantaneous time |
| $T_e$ | Torsional excitation |
| $\kappa$ | Shape coefficient for circular cross section |
| $\nu$ | Poisson's ratio |
| $\rho$ | Material density |
| $\varepsilon$ | Unbalance eccentricity |
| $\omega$ | Shaft spinning speed |
| $\omega_e$ | External excitation frequency |
| $\theta$ | Rotational angle of the rotor |
| $x,\eta,\xi$ | Rotor-fixed rotating coordinate system |
| $x,y,z$ | Inertial coordinate system |

## MODEL OF THE CRACKED SHAFT ELEMENT

Figure 1 shows a shaft element with a transverse crack of depth $a$, at distance $x$ from node 1, loaded with axial forces $P_1$, $P_7$, shear forces $P_2$, $P_3$, $P_8$, $P_9$, bending moments $P_5$, $P_6$, $P_{11}$, $P_{12}$, and torsional moments $P_4, P_{10}$. All six degrees of freedom per node are considered.

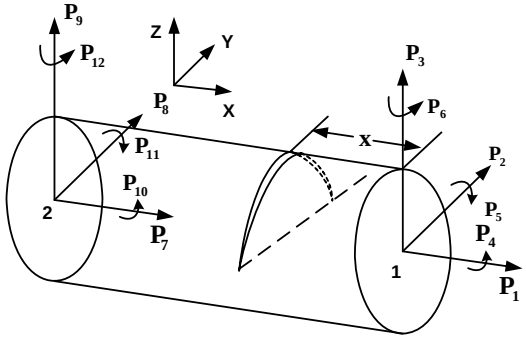


**Figure 1. Cracked shaft element in general loading.**

Since the strain energy induced at the tip of the loaded crack introduces the considerable local flexibility in the specific cracked beam element, the crack affects only the stiffness matrix of the given finite element. The geometry of shaft section with partially open crack is shown in Fig. 2, where $a$ is the depth of the fully open crack and $b$ is the half-width of the crack.

The node displacement in the direction of load $P_i$, induced only due to the presence of the crack with depth $\alpha$, can be

calculated as follows [19]:

$$u_i^c = \frac{\partial}{\partial P_i}\left[\int_A J(A)\,dA\right] \tag{1}$$

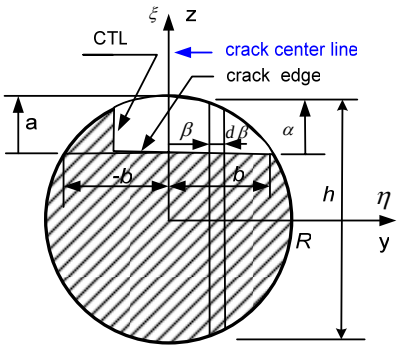


**Figure 2. Geometry of the shaft section with partially open crack.**

where $A$ is the area of the cracked section of the shaft (see Figure 2) and $J$ is the Strain Energy Density Function expressed as [21]:

$$J(A) = \frac{1}{E}\left[\left(\sum_{i=1}^{6} K_{Ii}\right)^2 + \left(\sum_{i=1}^{6} K_{IIi}\right)^2 + (1+\nu)\left(\sum_{i=1}^{6} K_{IIIi}\right)^2\right] \tag{2}$$

Here, $E$ is the modulus of elasticity, $\nu$ is the Poisson ratio, $K_{ij}$ are the crack Stress Intensity Factors (SIF) for $i$ = I, II, III crack displacement modes and load index $j$ = 1,2,…,6.

For a strip of unit thickness with a transverse crack the values of SIF are known [19] and thus, employing integration along the tip of the crack with the variable crack depth, yields the approximate values for SIF in Eq. (2). Based on Eq. (1), the local flexibility due to the crack is calculated as [22]:

$$c_{ij} = \frac{\partial^2}{\partial P_i \partial P_j}\left[\int_A J(A)\,dA\right] \tag{3}$$

The expressions for terms of the total flexibility matrix of the cracked element $\mathbf{c}_c = \left[c_{ij}\right]$ ($i,j$ =1,2,...,6) are given in Appendix A.

## MODEL OF THE CRACK BREATHING ACTION

For the majority of rotating machinery, the static deflection is much larger than the rotor's vibration amplitude. Under this assumption, the instantaneous shaft angular position can be employed to determine the amount of crack opening. Two extreme scenarios exist when the crack is either closed ($\theta = 0$) or open ($\theta = \pi$). For the spinning rotor at constant speed, a truly breathing crack behavior is represented by gradual opening of the crack from its fully closed to the fully open state and visa-versa. Since the flexibility of the cracked shaft section changes with different amount of crack opening, the concept of Crack Transition Line (CTL) is introduced. The CTL, which separates the open and closed portions of the crack, as illustrated in Fig. 2, is an imaginary line perpendicular to the crack edge. The integration limits for evaluation of flexibility coefficients depend on the amount of crack opening.

The crack edge is divided into ($N$+1) points. For any shaft angular position $\theta = i\left(180^\circ/N\right)$, the CTL is located at $\bar{b} - 2i\bar{b}/N$ $(i = 0...N)$ along the crack edge. The terms of flexibility matrix are continuously updated for each angle $\theta = 180^\circ/N$. In this way CTL keeps changing with different angles of shaft rotation, and thus reflecting the true crack "breathing" action.

The stiffness matrix for the shaft cracked element in the rotor-fixed coordinates system is calculated as:

$$\left[k_{mn}\right]_i = \left[c_{mn}\right]_i^{-1} \qquad m,n = 1,2,...,6;\ i = 0...N \tag{4}$$

where formulas for $\left[c_{mn}\right]_i$ are given in Appendix A.

In order to ensure the effectiveness of simulation, the variation of the cracked element stiffness with time (angular position), can be expressed by the truncated cosine series [23]:

$$\mathbf{k}_c = \mathbf{k}_0 + \sum_{i=1}^{4} \mathbf{k}_i \cos(i\omega t) \tag{5}$$

The coefficient stiffness matrices $\mathbf{k}_j$, $j = 0,1,...4$, are calculated based on the assumed amount of the crack's opening at its specific (five) angular positions.

Let define that stiffness matrices $\mathbf{k}_{uc}$, $\mathbf{k}_q$, $\mathbf{k}_{2q}$, $\mathbf{k}_{3q}$, and $\mathbf{k}_{op}$ to correspond to the rotor angular location at 0, $\pi/4$, $\pi/2$, $3\pi/4$, and $\pi$, respectively. They are calculated by assigning value of $i = 0$, $N/4$, $N/2$, $3N/4$, and $N$, respectively, in Eqs. (A2), i.e., by solving the following set of equations:

$$\mathbf{k}_c\big|_{\omega t=0} = \mathbf{k}_{uc},\quad \mathbf{k}_c\big|_{\omega t=\frac{\pi}{4}} = \mathbf{k}_q,\quad \mathbf{k}_c\big|_{\omega t=\frac{\pi}{2}} = \mathbf{k}_{2q}$$
$$\mathbf{k}_c\big|_{\omega t=\frac{3\pi}{4}} = \mathbf{k}_{3q},\ \mathbf{k}_c\big|_{\omega t=\pi} = \mathbf{k}_{op} \tag{6}$$

As a result, the fitting coefficient matrices take the following form:

$$\mathbf{k}_0 = \frac{\mathbf{k}_{2q}}{4} + \frac{\mathbf{k}_{uc}}{8} + \frac{\mathbf{k}_{op}}{8} + \frac{\mathbf{k}_q}{4} + \frac{\mathbf{k}_{3q}}{4}$$
$$\mathbf{k}_1 = \frac{1}{4}\left(\mathbf{k}_{uc} - \mathbf{k}_{op} + \sqrt{2}\mathbf{k}_q - \sqrt{2}\mathbf{k}_{3q}\right)$$
$$\mathbf{k}_2 = \frac{1}{4}\left(-2\mathbf{k}_{2q} + \mathbf{k}_{uc} + \mathbf{k}_{op}\right) \tag{7}$$
$$\mathbf{k}_3 = \frac{1}{4}\left(\mathbf{k}_{uc} - \mathbf{k}_{op} - \sqrt{2}\mathbf{k}_q + \sqrt{2}\mathbf{k}_{3q}\right)$$
$$\mathbf{k}_4 = \frac{\mathbf{k}_{2q}}{4} + \frac{\mathbf{k}_{uc}}{8} + \frac{\mathbf{k}_{op}}{8} - \frac{\mathbf{k}_q}{4} - \frac{\mathbf{k}_{3q}}{4}$$

The developed method predicts very well the variations of all terms of cracked element stiffness matrix due to the "breathing" action of the crack, over one shaft revolution (see Fig. 3[1]). Papadopoulos and Dimarogonas [17, 23] proposed similar approach but they assumed that the stiffness terms reach minimum values for the fully open crack, which is correct for

[1] Figure 3 is shown in Appendix B.

diagonal coefficients ( $k_{ii}$, $i=1,...,6$ ) but not for all cross-coupled terms. Some of the cross-coupled stiffness coefficients reach maximum or minimum values when the crack is half-open or half-closed, and become zero when the crack is fully open (see Fig. 3).

From the finite element static equilibrium conditions, 12 degrees of freedom of one element can be written as

$$\left(q_1, q_2, ..., q_{12}\right)^T = \mathbf{T}\left(q_1, q_2, ..., q_6\right)^T \tag{8}$$

where

$$\mathbf{T} = \begin{bmatrix} & & & \mathbf{I}_{6\times 6} & & \\ \hline -1 & 0 & 0 & 0 & 0 & 0 \\ 0 & -1 & 0 & 0 & 0 & 0 \\ 0 & 0 & -1 & 0 & 0 & 0 \\ 0 & 0 & 0 & -1 & 0 & 0 \\ 0 & 0 & -l & 0 & -1 & 0 \\ 0 & l & 0 & 0 & 0 & -1 \end{bmatrix} \tag{9}$$

Next, the stiffness of the cracked element in inertial coordinates system can be found as

$$\mathbf{K}_c = \mathbf{T}\mathbf{T}_e^T \mathbf{k}_c \mathbf{T}_e \mathbf{T}^T \tag{10}$$

where $\mathbf{T}_e$ is the transformation matrix from rotor-fixed coordinates system to the inertial coordinates system

$$\mathbf{T}_e = \begin{pmatrix} \mathbf{T}_a & \mathbf{0} \\ \mathbf{0} & \mathbf{T}_a \end{pmatrix} \tag{11}$$

and:

$$\mathbf{T}_a = \begin{pmatrix} 1 & 0 & 0 \\ 0 & \cos(\omega t) & \sin(\omega t) \\ 0 & -\sin(\omega t) & \cos(\omega t) \end{pmatrix} \tag{12}$$

When assembling the global stiffness matrix for the shaft, the cracked element stiffness matrix $\mathbf{K}_c$ replaces the stiffness matrix of the corresponding uncracked element. The equations of motion for the complete rotor system in an inertial coordinates system take the following form:

$$\mathbf{M}\ddot{\mathbf{q}} + \mathbf{C}\dot{\mathbf{q}} + \mathbf{K}(\omega t)\mathbf{q} = \mathbf{F} \tag{13}$$

where **M**, **C,** and $\mathbf{K}(\omega t)$ are the mass, damping and stiffness matrices, respectively, for the whole rotor system. The stiffness matrix is continuously updated with the angular position $\omega t$ of the shaft. The force vector **F** can contain any kind of forces and moments applied at any nodes in the global inertial coordinate system.

## NUMERICAL SIMULATIONS

A two-disk rotor system considered for numerical studies is shown in Fig. 4. Physical parameters of the model are listed in Table 1. The boundary conditions for the model follow the same conditions as for simply supported beam except constrain imposed on torsional degree of freedom at the right support. The shaft is divided into 8 equal-length finite elements and two shown cracks shown are located at element 6 and 7, near the right disk (see Fig. 4).

**Table 1: Numerical Model Physical Parameters.**

| | Physical parameter | Value | Units |
|---|---|---|---|
| $L$ | Shaft length | 1.12 | m |
| $D$ | Shaft diameter | 0.03 | m |
| $\rho$ | Material density | 7750 | $Kg/m^3$ |
| $\nu$ | Poisson's ratio | 0.3 | |
| $E$ | Modulus of elasticity | $2.07\times10^{11}$ | $N/m^2$ |
| $G$ | Shear modulus of elasticity | $7.96\times10^{10}$ | $N/m^2$ |
| $M$ | Disk mass | 3 | kg |
| $J_P$ | Disk polar moment of inertia | 0.018 | $kg\ m^2$ |
| $J_D$ | Diametral moment of inertia | 0.01 | $kg\ m^2$ |
| $\varepsilon$ | Unbalance eccentricity | $5.4\times10^{-5}$ | m |

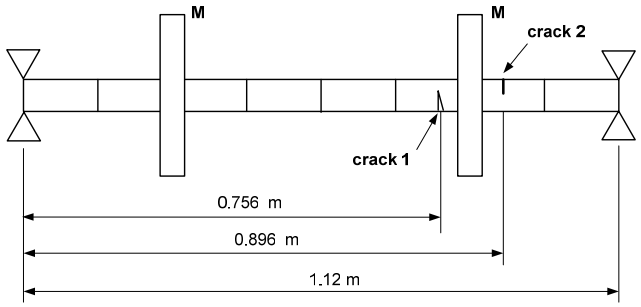


**Figure 4. A two-disk rotor system with two cracks near the right disk.**

### Frequency Analysis

Frequency analysis is carried out for an undamped non-rotating rotor. Three cases are considered for the cracks located at different axial locations, different phases, depth, and shaft geometric ratios.

*Case*1:

Two open cracks of depths of $a_1/D = a_2/D = 0.4$; the position of one crack is fixed (0.756 m from the left support, see Fig. 4) while the position of the other one keeps changing from the left to right end.

The variation of the first two mode frequencies, as a function of axial position of the second crack, is illustrated in Fig. 5(a). When the second crack is near the ends of the rotor the frequencies are almost the same as for the rotor with only one crack. The effect of the second crack on the rotor first two mode frequencies gradually increases, reaching the maximum as the crack's position approaches the middle of the shaft.

The third mode frequency, shown in Fig. 5(b), predominantly torsional, is very little affected by the position of the second crack. One can observe that when this position is between the left support and the left disk, the mode frequency is almost identical as for the rotor with one crack, i.e., 598 rad/s. For the position anywhere between two disks, the frequency drops to 595 rad/s, and for the position between right

disk and the right support the frequency is reduced further to 591.5 rad/s.

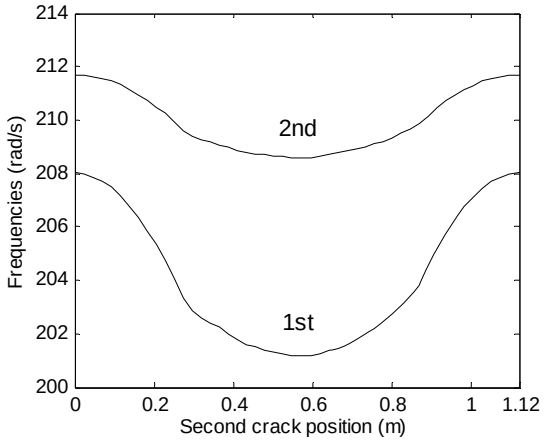


(a)

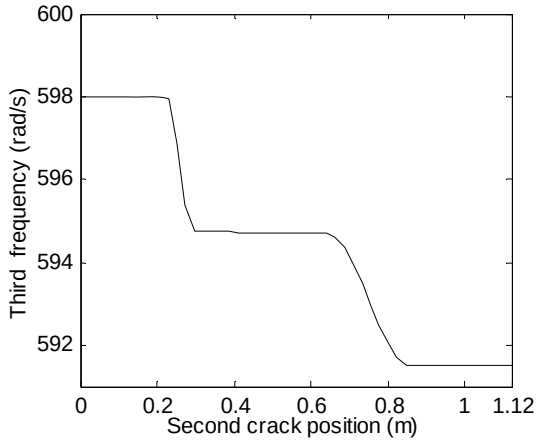


(b)

**Figure 5. Variation of mode frequencies for various positions of the second crack: (a) first two mode frequencies, and (b) third mode frequency.**

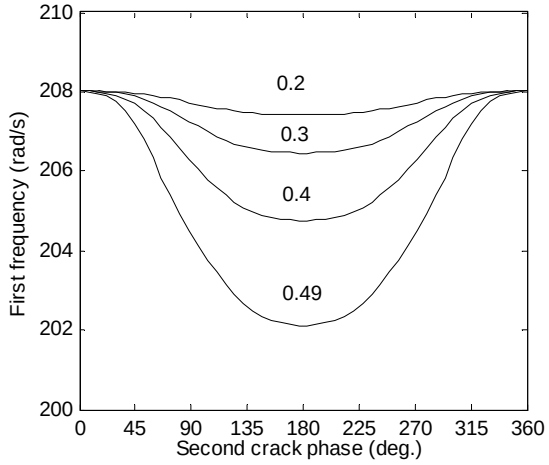


(a)

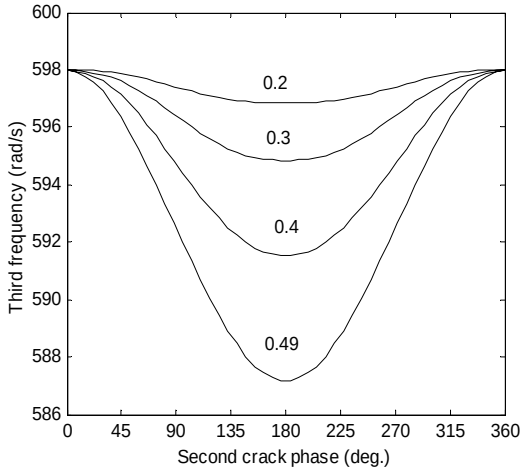


(b)

**Figure 6. Variation of mode frequencies for various values of phase and depth of second crack: (a) first mode frequency, and (b) third mode frequency.**

*Case* 2:

Two cracks have fixed axial positions; one crack at the distance 0.756 m and the second one at 0.896 m, measured from the left support (see Fig. 4). The first crack, of fixed depth $a_1/D = 0.4$, is always open, while the second is allowed to be oriented at any angle (phase) with respect to the positive *z*-axis, and have different depths. The changes of rotor mode frequencies with different depths and angular position of the second crack are illustrated in Fig. 6. It should be noted that the crack center line is defined as a line perpendicular to the crack edge, and here, the crack phase angle is defined as the angle between the positive *z*-axis and the crack's centerline (see Fig. 2). As expected, that the maximum reduction of frequencies happens to be when both cracks are fully open (phase 180°). Also, with the growing depth of the second crack, the rotor frequency reduction becomes more significant.

*Case* 3:

Two cracks are located at fixed axial positions. Both cracks have fixed depths ($a_1/D = a_2/D \equiv 0.4$), but the shaft has different geometric ratios, i.e., for the given length of the shaft ($L$ = 1.12 m) the shaft diameter is varied ($D$ = 0.2, 0.08, 0.06, 0.04, 0.02 m). Also, the phase of the second crack keeps changing. As can be seen on Fig. 7(a), the third, predominantly torsional mode frequency is not much affected by the crack's phase. To emphasize the scale of possible changes Figs. 7(b) and 7(c) show changes of the normalized frequency (with respect to its maximum value). For the rotor with smaller geometric ratios (i.e., larger shaft diameter), the variation of the frequencies is more sensitive to the phase change of the crack.

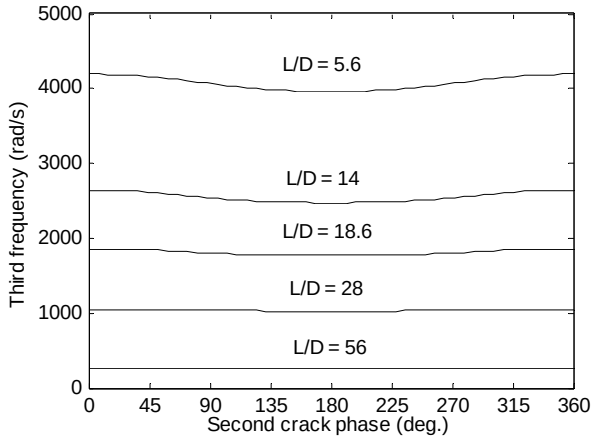


(a)

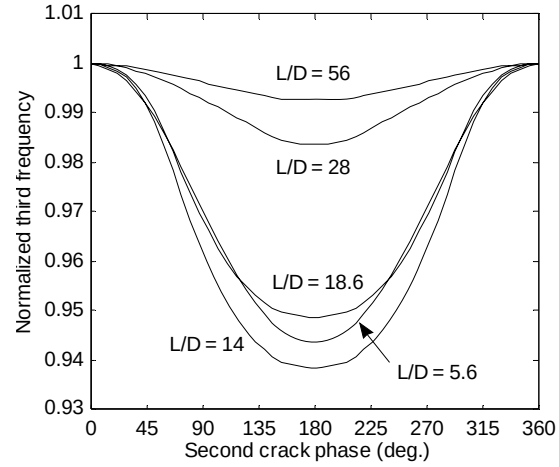


(b)

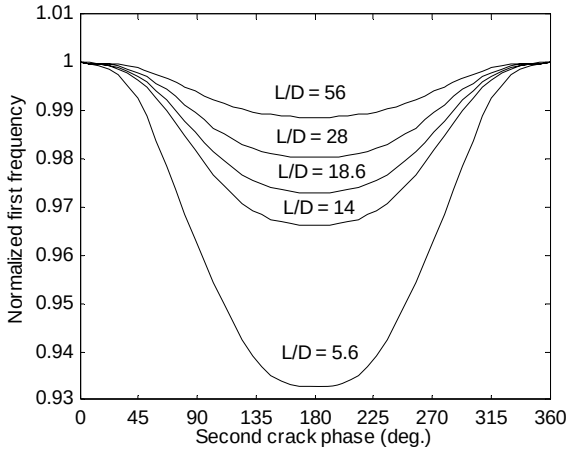


(c)

**Figure 7. Variation of mode frequencies for different shaft geometric ratios: (a) variation of the third mode frequency (b) variation of the normalized frequency for the third mode, (c) variation of the normalized frequency for the first mode.**

**Lateral and Torsional Vibration Response**

In this part of investigation two breathing cracks (rotating rotor) located at element 6 and 7 have the same depth $a_1/D = a_2/D \equiv 0.4$. The stiffness variation property of the cracked element has been described in the previous section. The bending and torsional frequencies of the uncracked rotor are 214.4 rad/s and 601.3 rad/s, respectively.

In order to explore the crack-induced mode coupling phenomenon, an external sinusoidal excitation torque $T_e = 600\sin(\omega_e t)$ is applied at the first disk (node 3), with $\omega_e = 322$ rad/s as an excitation frequency. The selected shaft spinning speed is $\omega = 43$ rad/s. The purpose is to investigate how the torsional excitation affects the lateral vibration response of cracked rotor. Vibration responses for the three different phases of the two cracks are shown in Fig. 8[2].

In all these plots of Fig. 8, the existence of the first harmonic (1X) and super-harmonics (2X, 3X, 4X,) of the shaft running frequency in lateral frequency spectrum provide strong indication of the cracks' presence. One can also notice the existence of torsional frequency, $\omega_e$, in the lateral frequency spectrum, which clearly demonstrates the coupling mechanism between the lateral and torsional vibration modes. The appearance of sum and difference frequencies $(\omega_e \pm n\omega)$ around the torsional excitation frequency is the result of interaction of the torsional excitation and the synchronous frequency and its higher harmonics (2X, 3X, 4X).

For the case with cracks' phase difference of 0°, shown in Fig. 8(a) and 8(b), the two cracks simultaneously open or close during the rotor's rotation.. In this case the vibration spectrum of the two-crack rotor is similar to the one-crack rotor's behavior, except the increased amplitude due to higher stiffness reduction.

For the case with phase difference of $90^\circ$, shown in Fig. 8(c) and 8(d), whenever one crack is closed, the other one is always half-opened and half-closed. While 2X, 3X and 5X peaks remain about the same, as in Fig. 8(a) and 8(b), the amplitude of 4X peak is dramatically decreased in the frequency spectra, and the vibration amplitude is slightly reduced.

The third case with the phase difference of $180^\circ$ implies that whenever one crack is fully opened, the other one must be closed. In this case the vibration amplitudes are reduced further than in the previous case. Although the super-harmonic 2X and 4X peaks are similar as in Fig. 8(a) and 8(b), 1X, 3X and 5X peaks are appreciable decreased to their minimum values.

Due to the lateral and torsional coupling mechanism induced by the presence of cracks, the externally applied torsional excitation significantly affects the rotor lateral vibration behavior. This is clearly shown in Figs. 9[3] (a) and (b), where the vibration response orbits are presented without and with torque, respectively. The Fig. 9(b) shows the orbit that rotates (thin line) in the opposite direction of the rotor's rotating direction. Simulations of orbits considering frequencies shown in corresponding to this case FFT spectrum (see Fig. 8(b)) have shown presence of frequency components being backward whirl fraction. The vibration in the presence of the applied external torque is not periodic but quasi-periodic, where the ratios of the involved frequencies are not the ratios of integers.

[2] Figure 8 is shown in Appendix B.
[3] Figure 9 is shown in Appendix B.

## CONCLUSIONS

Coupled lateral-torsional vibration finite element analysis of a rotor with two breathing cracks has been conducted for frequency analysis and dynamic response to excitation forces such as mass unbalance, weight, and the external torque. The multi-crack rotors have much more complicated stiffness asymmetry behavior being parametric, time-varying systems with dissimilar inertia moments in two perpendicular directions and at various axial shaft locations. The issue of accurate modeling of the stiffness matrix with the periodic coefficients in the global inertial coordinates system is crucial to account for the proper breathing behavior of multi cracks located at various axial and angular positions.

The developed model for the "breathing" cracked element is based on fracture mechanics. The direct stiffnesses, as well as cross coupling stiffnesses are estimated as the crack opens and closes. The stiffness matrix variation due to the crack breathing is determined by the stiffness matrices of cracked shaft with the crack located at five different angular positions. Such an approach simplifies frequency and dynamic response analysis regardless of a number of finite elements and cracks' location.

The axial location of cracks affects the rotor frequencies. Once the two cracks are located close to the middle section of the shaft, the maximum reduction of frequencies occurs. The frequencies also depend on the relative orientation of two cracks and the shaft geometric ratios. The variation of rotor mode frequencies is the most significant for the small shaft geometric ratios. The modes which affected the most are predominantly bending modes. If the two breathing cracks are in phase, i.e., both of them are simultaneously either opened or closed, the vibration behavior pattern is almost the same as for the rotor with one crack, except the change in vibration amplitude. For the case of two out-of-phase cracks, the vibration spectrum presents different signatures, with diminished 1X, 3X and 5X harmonics. Finally, for the cracks' phase difference of 90°, the peak of super-harmonic frequency 4X is dramatically reduced in the vibration spectrum. It is noteworthy that the 2X peak stays the same all the time.

The orbit analysis reveals that there are specific crack signatures due to the vibration mode coupling. When the external torque is applied the mode coupling induced by the crack causes vibration to become quasi-periodic, with the response orbit rotating in the direction opposite to the direction of rotation of the rotor.

The presented method is applicable to analyze the dynamic response of rotating shafts with two or more breathing cracks. The uniqueness of the observed crack signatures, captured by the analytical approach, presents potential in early diagnosis of rotor cracks.

## ACKNOWLEDGMENTS

This research was conducted under grant NAG 3-2573 of the NASA Glenn Research Center. This support is gratefully acknowledged.

## REFERENCES

[1] Sawicki, J.T., 2002, "Some Advances in Diagnostics of Rotating Machinery Malfunctions," Invited Paper, International Symposium on Machine Condition Monitoring and Diagnosis, Annual Meeting of the Japan Society of Mechanical Engineers, Tokyo.

[2] Tondl, A., 1965, *Some Problems of Rotor Dynamics*, Chapman & Hall, London.

[3] Wauer, J., 1990, "On the Dynamics of Cracked Rotors: A Literature Survey," *Applied Mechanics Reviews*, **43**(1), pp. 13-17.

[4] Papadopoulos, P. and Dimarogonas, A.D., 1987, "Coupling of Bending and Torsional Vibration of a Cracked Timoshenko Shaft," Ingenieur-Archive, **57**, pp. 257-266.

[5] Plaut, R.H. and Wauer, J., 1995, "Parametric, External and Combination Resonances in Coupled Flexural and Torsional Oscillations of an Unbalanced Rotating Shaft," *Journal of Sound and Vibration*, **183**(5), pp. 889-897.

[6] Muszynska, A., Goldman, P., and Bently, D.E., 1992, "Torsional/Lateral Vibration Cross-Coupled Responses Due to Shaft Anisotropy: A New Tool in Shaft Crack Detection," 5th International Conference on Vibrations in Rotating Machinery, Bath, U.K., Paper C432/090, pp. 257-262.

[7] Bently, D. E., Goldman, P. and Muszynska, A., 1997, ""Snapping" Torsional Response of an Anisotropic Radially Loaded Rotor," *Journal of Engineering for Gas Turbines and Power*, **119**, pp. 397-403.

[8] Gasch, R., Markert, R., and Pfutzner, H., 1979, "Acceleration of Unbalanced Flexible Rotors through the Critical Speeds," *Journal of Sound and Vibration*, **63**, pp. 393-409.

[9] Sawicki, J.T., Wu, X., Baaklini, G., and Gyekenyesi, A.L., 2003, "Vibration-Based Crack Diagnosis in Rotating Shafts During Acceleration through Resonance," *Proceedings of SPIE 10th Annual International Symposium on Smart Structures and Materials*, San Diego, California.

[10] Sawicki, J.T., Bently, D.E., Wu, X., Baaklini, G., and Friswell, M.I., 2003, "Dynamic Behavior of Cracked Flexible Rotor Subjected to Constant Driving Torque," *Proceedings of the 2nd International Symposium on Stability Control of Rotating Machinery*, Gdansk, Poland, pp. 231-241.

[11] Henry, T. A. and Okah-Avae, B. E., 1976, "Vibrations in Cracked Shafts," Paper C162/76, *I.Mech.E. Conference on Vibrations in Rotating Machinery*, pp. 15-19.

[12] Mayes, I. W. and Davies, W. G. R., 1976, "The Vibration Behavior of a Rotating Shaft System Containing a Transverse Crack," Paper C168/76, *I.Mech.E. Conference on Vibrations in Rotating Machinery*, pp. 53-64.

[13] Gasch, R., 1976, "Dynamic behavior of a simple rotor with a cross-sectional crack," Paper C178/76, *I. Mech. E. Conference on Vibrations in Rotating Machinery*, pp.123-128.

[14] Gasch, R. A, 1993, "Survey of the Dynamic Behavior of a Simple Rotating Shaft with a Transverse Crack," *Journal of Sound and Vibration*, **160**, pp. 313-332.

[15] Mayes, I. W. and Davies, W. G. R., 1984, "Analysis of the Response of a Multi-Rotor-Bearing System Containing a Transverse Crack in a Rotor," *ASME Journal of Vibration, Acoustics, Stress, and Reliability in Design*, **106**, pp. 139-145.

[16] Collins, K.R., Plaut, R.H., and Wauer, J., 1991, "Detection of Cracks in Rotating Timoshenko Shafts Using Axial Impulses," *ASME Journal of Vibration and Acoustics*, **113**, pp. 74-78.
[17] Papadopoulos, C. A., and Dimarogonas, A. D., 1987, "Coupled Longitudinal and Bending Vibrations of a Rotating Shaft with an Open Crack," *Journal of Sound and Vibration*, **117**, pp. 81–93.
[18] Papadopoulos, C. A., and Dimarogonas, A. D., 1992, "Coupled Vibration of Cracked Shafts," *ASME Journal of Vibration and Acoustics*, Vol. 114, pp. 461-467.
[19] Sekhar, A. S., 1999, "Vibration Characteristics of a Cracked Rotor with Two Open Cracks," *Journal of Sound and Vibration*, **223**(4), pp. 497-512.
[20] Darpe, A. K., Gupta, K. and Chawla, A., 2004, "Coupled Bending, Longitudinal and Torsional Vibrations of a Cracked Rotor," *Journal of Sound and Vibration*, **269**, pp. 33-60.
[21] Tada, H., Paris, P. C. and Irwin, G. R., 1973, *The Stress Analysis of Cracks Handbook*, Del Research Corporation, Hellertown, PA.
[22] Dimarogonas, A. D., and Papadopoulos, C. A., 1983, *Analytical Methods in Rotor Dynamics*, Applied Science Publishers, London.
[23] Papadopoulos, C. A., and Dimarogonas, A. D., 1988, "Stability of Cracked Rotors in the Coupled Vibration Mode," *ASME Journal of Vibration, Acoustics, Stress, and Reliability in Design*, **110**, pp. 357-359.

## APPENDIX A
## Terms of flexibility matrix

$$I_{c1i}=\frac{1}{\pi ER}\int_{\bar{b}-\frac{2i\bar{b}}{N}}^{\bar{b}}\int_{0}^{\bar{a}-1+\sqrt{1-\bar{\beta}^2}} 2\bar{\alpha}F_1^2\left(\bar{\alpha},\bar{\beta}\right)d\bar{\alpha}d\bar{\beta}$$

$$I_{c2i}=\frac{1}{\pi ER^2}\int_{\bar{b}-\frac{2i\bar{b}}{N}}^{\bar{b}}\int_{0}^{\bar{a}-1+\sqrt{1-\bar{\beta}^2}} 8\bar{\alpha}\sqrt{1-\bar{\beta}^2}F_1\left(\bar{\alpha},\bar{\beta}\right)F_2\left(\bar{\alpha},\bar{\beta}\right)d\bar{\alpha}d\bar{\beta}$$

$$I_{c3i}=\frac{1}{\pi ER^2}\int_{\bar{b}-\frac{2i\bar{b}}{N}}^{\bar{b}}\int_{0}^{\bar{a}-1+\sqrt{1-\bar{\beta}^2}} 8\bar{\alpha}\bar{\beta}F_1^2\left(\bar{\alpha},\bar{\beta}\right)d\bar{\alpha}d\bar{\beta} \qquad \text{(A1)}$$

$$I_{c4i}=\frac{1}{\pi ER}\int_{\bar{b}-\frac{2i\bar{b}}{N}}^{\bar{b}}\int_{0}^{\bar{a}-1+\sqrt{1-\bar{\beta}^2}} 2\kappa^2\bar{\alpha}F_{II}^2\left(\bar{\alpha},\bar{\beta}\right)d\bar{\alpha}d\bar{\beta}$$

$$I_{c5i}=\frac{1}{\pi ER^3}\int_{\bar{b}-\frac{2i\bar{b}}{N}}^{\bar{b}}\int_{0}^{\bar{a}-1+\sqrt{1-\bar{\beta}^2}} 32\bar{\alpha}\left(1-\bar{\beta}^2\right)F_2^2\left(\bar{\alpha},\bar{\beta}\right)d\bar{\alpha}d\bar{\beta}$$

$$I_{c6i}=\frac{1}{\pi ER^3}\int_{\bar{b}-\frac{2i\bar{b}}{N}}^{\bar{b}}\int_{0}^{\bar{a}-1+\sqrt{1-\bar{\beta}^2}} 32\bar{\alpha}\bar{\beta}\sqrt{1-\bar{\beta}^2}F_1\left(\bar{\alpha},\bar{\beta}\right)F_2\left(\bar{\alpha},\bar{\beta}\right)d\bar{\alpha}d\bar{\beta}$$

$$I_{c7i}=\frac{1}{\pi ER^2}\int_{\bar{b}-\frac{2i\bar{b}}{N}}^{\bar{b}}\int_{0}^{\bar{a}-1+\sqrt{1-\bar{\beta}^2}} 4\kappa\bar{\alpha}\bar{\beta}F_{II}^2\left(\bar{\alpha},\bar{\beta}\right)d\bar{\alpha}d\bar{\beta}$$

$$I_{c8i}=\frac{1}{\pi ER^3}\int_{\bar{b}-\frac{2i\bar{b}}{N}}^{\bar{b}}\int_{0}^{\bar{a}-1+\sqrt{1-\bar{\beta}^2}} 32\bar{\alpha}\bar{\beta}^2F_1^2\left(\bar{\alpha},\bar{\beta}\right)d\bar{\alpha}d\bar{\beta}$$

$$I_{c9i}=\frac{1}{\pi ER}\int_{\bar{b}-\frac{2i\bar{b}}{N}}^{\bar{b}}\int_{0}^{\bar{a}-1+\sqrt{1-\bar{\beta}^2}} 2m\kappa^2\bar{\alpha}F_{III}^2\left(\bar{\alpha},\bar{\beta}\right)d\bar{\alpha}d\bar{\beta}$$

$$I_{c10i}=\frac{1}{\pi ER^2}\int_{\bar{b}-\frac{2i\bar{b}}{N}}^{\bar{b}}\int_{0}^{\bar{a}-1+\sqrt{1-\bar{\beta}^2}} 4m\kappa\bar{\alpha}\sqrt{1-\bar{\beta}^2}F_{III}^2\left(\bar{\alpha},\bar{\beta}\right)d\bar{\alpha}d\bar{\beta}$$

$$I_{c11i}=\frac{1}{\pi ER^3}\int_{\bar{b}-\frac{2i\bar{b}}{N}}^{\bar{b}}\int_{0}^{\bar{a}-1+\sqrt{1-\bar{\beta}^2}} 8\bar{\alpha}\bar{\beta}^2F_{II}^2\left(\bar{\alpha},\bar{\beta}\right)d\bar{\alpha}d\bar{\beta}$$

$$I_{c12i}=\frac{1}{\pi ER^3}\int_{\bar{b}-\frac{2i\bar{b}}{N}}^{\bar{b}}\int_{0}^{\bar{a}-1+\sqrt{1-\bar{\beta}^2}} 8m\bar{\alpha}\left(1-\bar{\beta}^2\right)F_{III}^2\left(\bar{\alpha},\bar{\beta}\right)d\bar{\alpha}d\bar{\beta}$$

where:

$$F_1\left(\frac{\alpha}{h}\right)=\sqrt{\frac{\tan\lambda}{\lambda}}\,\frac{0.752+2.02\left(\alpha/h\right)+0.37\left(1-\sin\lambda\right)^3}{\cos\lambda}$$

$$F_2\left(\frac{\alpha}{h}\right)=\sqrt{\frac{\tan\lambda}{\lambda}}\,\frac{0.923+0.199\left(1-\sin\lambda\right)^4}{\cos\lambda}$$

$$F_{II}\left(\frac{\alpha}{h}\right)=\frac{1.122-0.561\left(\alpha/h\right)+0.085\left(\alpha/h\right)^2+0.18\left(\alpha/h\right)^3}{\sqrt{1-\alpha/h}}$$

$$F_{III}\left(\frac{\alpha}{h}\right)=\sqrt{\frac{\tan\lambda}{\lambda}},\quad \lambda=\frac{\pi\alpha}{2h},\quad \kappa=\frac{6\left(1+\nu\right)}{\left(7+6\nu\right)},\quad h=2\sqrt{R^2-\beta^2}$$

$$\bar{a}=\frac{a}{R},\quad \bar{b}=\sqrt{2\bar{a}-\bar{a}^2},\quad \bar{\alpha}=\frac{\alpha}{R}=\bar{a}-1+\sqrt{1-\bar{\beta}^2}$$

$$\bar{\beta}=\frac{\beta}{R},\quad \bar{h}=\frac{h}{R}=2\sqrt{1-\bar{\beta}^2},\quad \lambda=\frac{\pi\bar{\alpha}}{4\sqrt{1-\bar{\beta}^2}}$$

$$\frac{\alpha}{h}=\frac{\bar{\alpha}}{2\sqrt{1-\bar{\beta}^2}},\quad i=0,1,2,...,N,\ m=1+\nu$$

and

$$c_{11}=\frac{l}{AE}+I_{c1i},\quad c_{12}=xI_{c2i},\quad c_{13}=xI_{c3i}$$

$$c_{14}=0,\quad c_{15}=I_{c3i},\quad c_{16}=-I_{c2i}$$

$$c_{21}=c_{12},\quad c_{22}=\frac{l^3}{3EI}+I_{c4i}+x^2I_{c5i}$$

$$c_{23}=x^2I_{c6i},\quad c_{24}=I_{c7i},\quad c_{25}=xI_{c6i},$$

$$c_{26} = -\frac{l^2}{2EI} - xI_{c5i},\ \ c_{31} = c_{13},\ \ c_{32} = c_{23}$$

$$c_{33} = \frac{l^3}{3EI} + I_{c9i} + x^2 I_{c8i},\ \ c_{34} = I_{c10i}$$

$$c_{35} = \frac{l^2}{2EI} + xI_{c8i},\ \ c_{36} = -xI_{c6i},\ c_{41} = 0$$

$$c_{42} = c_{24},\ \ c_{43} = c_{34},\ \ c_{44} = \frac{l}{GJ} + I_{c11i} + I_{c12i} \qquad \text{(A2)}$$

$$c_{45} = 0,\ \ c_{46} = 0,\ \ c_{51} = c_{15},\ \ c_{52} = c_{25}$$

$$c_{53} = c_{35},\ \ c_{54} = 0,\ \ c_{55} = \frac{l}{EI} + I_{c8i}$$

$$c_{56} = -I_{c6i},\ \ c_{61} = c_{16},\ \ c_{62} = c_{26},\ \ c_{63} = c_{36}$$

$$c_{64} = 0,\ \ c_{65} = c_{56},\ \ c_{66} = \frac{l}{EI} + I_{c5i}$$

## APPENDIX B

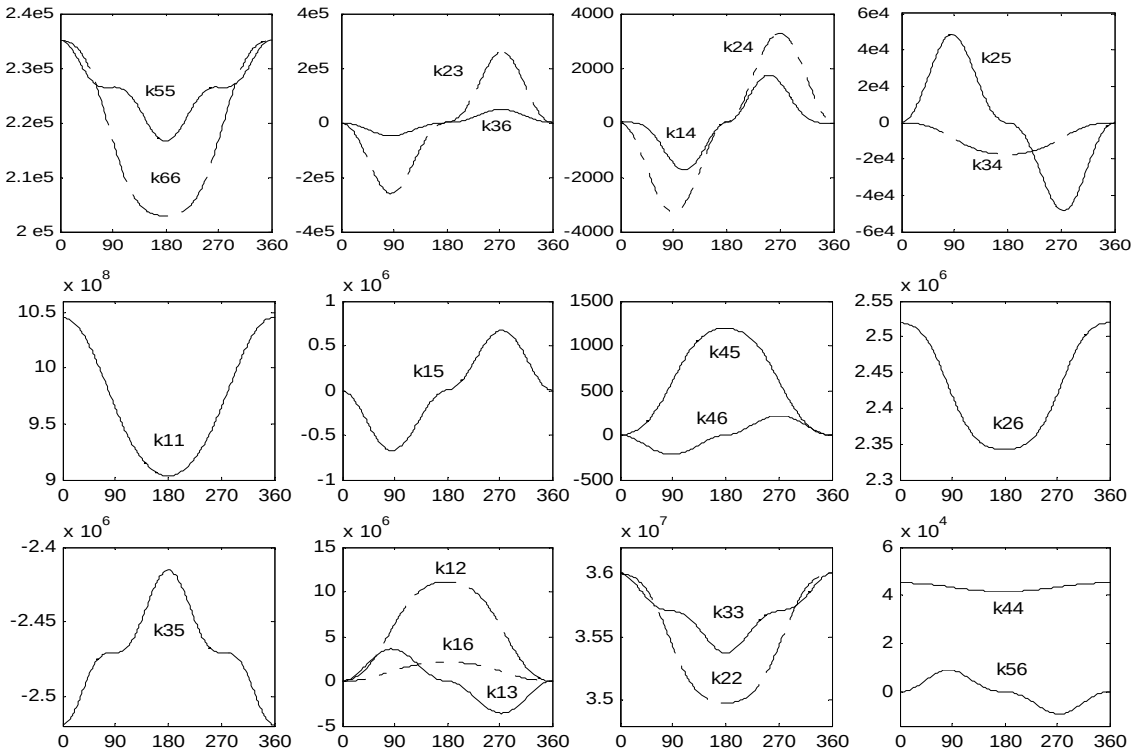


**Figure 3. Variation of stiffness coefficients over one revolution of a cracked shaft element (a/D = 0.4, l = 0.14m, D=0.03m).**

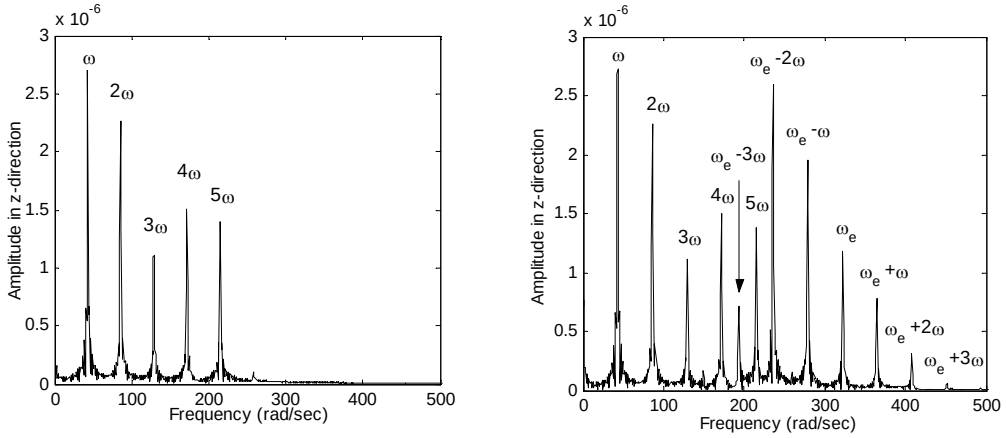


(a). Phase difference $0^\circ$ ; no torsional excitation.

(b). Phase difference $0^\circ$ ; torsional excitation

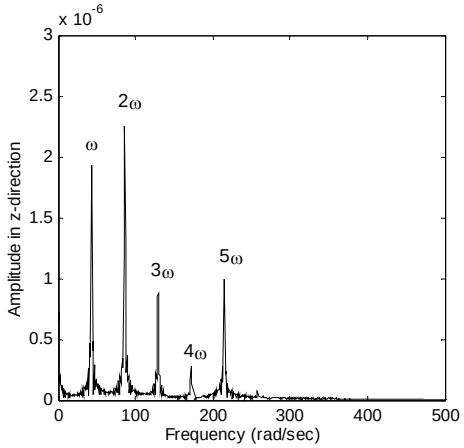


(c). Phase difference 90°; no torsional excitation.

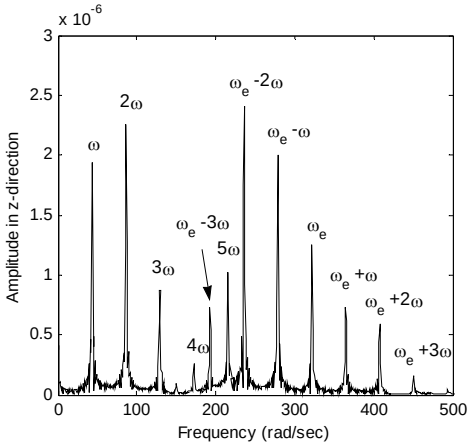


(d). Phase difference 90°; torsional excitation.

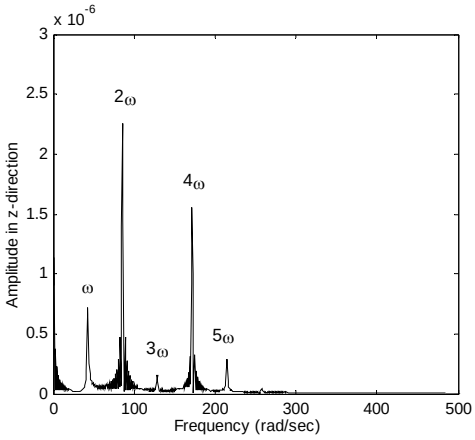


(e). Phase difference 180°; no torsional excitation.

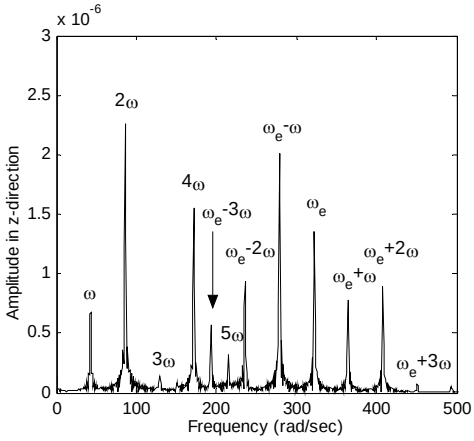


(f). Phase difference 180°; torsional excitation.

**Figure 8. Vibration response FFT of a rotor with two breathing cracks of different phase.**

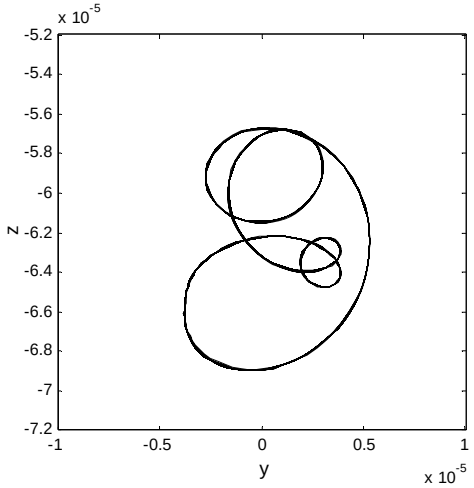


(a)

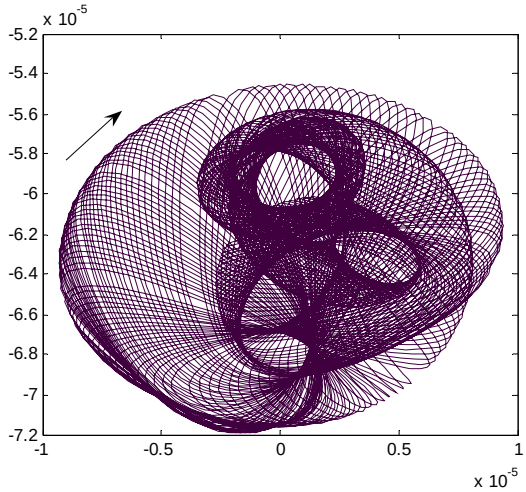


(b)

**Figure 9. Vibration response orbits with phase difference 0°: (a) without torsional excitation, (b) with torsional excitation.**